Journal of Applied Electrochemistry **34**: 715–722, 2004.

Preformed boehmite nanoparticles as coating materials for long-cycling $LiCoO_2$

G.T.K. FEY[1,*], Z.X. WENG[1], J.G. CHEN[1], C.Z. LU[1], T.P. KUMAR[1,3], S.P. NAIK[1], A.S.T. CHIANG[1], D.C. LEE[2] and J.R. LIN[2]
[1]*Department of Chemical and Materials Engineering, National Central University, Chung-Li, Taiwan 32054, R.O.C.*
[2]*Industrial Technology Research Institute, 195, Section 4, Chung Hsing Road, Hsin-chu, Taiwan 310, R.O.C.*
[3]*On deputation from: Central Electrochemical Research Institute, Karaikudi 630006, India*
*(*author for correspondence, e-mail: gfey@cc.ncu.edu.tw)*

Received 3 October 2003; accepted in revised form 13 January 2004

Key words: coated cathode, cyclability, $LiCoO_2$, lithium batteries, nanoparticulate coating

Abstract

A simple mechano-thermal coating procedure for the production of long-cycling $LiCoO_2$ is described. Preformed nanoparticulate boehmite was used as the coating material. The coating procedure resulted in the cathode particles covered in a 20–30 nm thick kernel of boehmite, as revealed by TEM examination. XRD studies showed that the lattice parameter *c* diminished upon coating, indicating that a substitutional compound of the composition $Li_xAl_yCo_{1-y}O_2$ may have formed upon calcination. SEM images, *R*-factor values from XRD studies and galvanostatic charge–discharge studies showed that a coating level of 1.0 wt % gave an optimal performance in capacity and cyclability. SEM images showed that above the 1.0 wt % coating level, the excess boehmite adhered to the coated cathode particles as sperules. ESCA depth profile analysis showed partial diffusion of aluminum from the surface to the interior. Galvanostatic cycling studies showed that at a coating level of 1.0 wt %, cyclability improved three- and twelve-fold for the two commercial $LiCoO_2$ samples tested. Cyclic voltammetry revealed that the hexagonal- monoclinic-hexagonal phase transformations during cycling were suppressed in the coated cathode materials.

1. Introduction

Thanks mainly to their superior performance characteristics, reliability and safety, lithium-ion batteries today power the majority of portable instruments such as laptop computers and cellular phones. The most popular cathode material in these batteries is $LiCoO_2$, isostructural with the rhombohedral α-$NaFeO_2$ [1]. The high electronegativity of oxygen results in repulsive interactions between adjacent oxygen layers, which are compensated for by the positive lithium and cobalt ions residing between the layers [2, 3]. Therefore, the removal of the electrically screening lithium ions from $LiCoO_2$ results in increased repulsion between the CoO_2 sheets. Thus, the deintercalation of lithium from $LiCoO_2$ results in an expansion of the hexagonal lattice in the *c*-direction [4, 5], and a contraction in the Co—Co distance [6, 7]. Extraction of more than 0.5 Li from $LiCoO_2$ can destabilize the structure. The anisotropic volume change during repeated cycling causes structural degradation of the host material [8], which results in serious capacity fade [9, 10]. The structural degradation is also thought to be closely associated with the dissolution of cobalt, seriously jeopardizing the cycle life of the cathode material [10].

Recently, several groups have attempted to circumvent this problem by coating $LiCoO_2$ particles with a thin film of oxide materials such as Al_2O_3 [11–14], MgO [14–16], SnO_2 [14, 16], TiO_2 [13] and ZrO_2 [13]. It was expected that surface modifications might lead to improved performance. Since the degradation of the cathode material appears to be related to surface defects or its surface chemistry [10], coating with an inert material can modify the surface and possibly influence the cycling performance [14]. Some authors suggest that the coating materials form substitutional oxides on the cathode surface, which bestow improved structural stability to the core material, enhancing its cyclability [16]. Cho et al. [13] suggest that coatings with high fracture-tough materials suppress the cycle-limiting phase transitions associated with the intercalation–deintercalation processes. The coating procedures adopted in most of the above studies were based on the sol–gel technique, in which the oxide formed by the hydrolysis of a metal alkoxide was deposited *in situ*, followed by a calcination step. In a departure from the conventional processes, we have adopted a simple process by which preformed nanoparticles of the coating material are deposited on cathode powders. In this paper, we describe the physico-chemical properties and

electrochemical cycling behaviour of $LiCoO_2$ coated with preformed boehmite nanoparticles by a simple mechano-thermal coating process.

2. Experimental details

A weighed amount of a commercial boehmite powder ($[AlO(OH)]_n$, DISPAL 18N4 from Condea Chemie, Germany) was dispersed in ethanol by a 1 h sonication followed by 10 h of vigorous stirring. A commercial sample of $LiCoO_2$ ($LiCoO_2$-A from Coremax Taiwan Corporation, surface area: 0.62 $m^2\ g^{-1}$; particle size: 1–5 μm; or $LiCoO_2$-B from Foote Mineral Corporation, surface area: 0.27 $m^2\ g^{-1}$; particle size: 3–10 μm) was added to this dispersion such that the weight ratios of the boehmite to the cathode material were 0.3:99.7, 1.0:99.0, 3.0:97.0 and 5.0:95.0. The mixture was sonicated for 30 min, and stirred on a magnetic stirrer for 24 h. A subsequent slow evaporation of the solvent at 50 °C resulted in a black dry mass of boehmite-coated $LiCoO_2$ particles. The coated particles were calcined at 450 °C for 10 h in order to ensure complete adhesion of the coated particles with the core material. The coating procedure is schematically represented in Figure 1.

An X-ray diffractometer (Siemens D-5000, Mac Science MXP18) equipped with a nickel-filtered CuK_α radiation source was used for structural analysis. The diffraction patterns were recorded between scattering angles of 5° and 80° in steps of 0.05°. BET surface area measurements were carried out on a Micromeritics ASAP 2010 surface area analyser at 77 K. Prior to the measurements, the boehmite sample was degassed for 12 h at 250 °C under 10^{-6} torr in order to remove absorbed moisture. Particle size of the coating material was determined by the dynamic light scattering (DLS) technique on a Malvern ZetaSizer-3000 with a 10 mW He–Ne laser. The sample for the DLS analysis was a dispersion of the boehmite in water, prepared by sonication for one hour. The surface morphology of the coated materials was examined by scanning electron microscopy (Hitachi model S-3500V). The microstructures of the coated particles were examined by a Jeol JEM-200FXII transmission electron microscope equipped with a LaB_6 gun. The samples for TEM studies were prepared by dispersing the coated powders in ethanol, placing a drop of the clear solution on a carbon-coated copper grid, and subsequent drying. Depth profiles of aluminium, cobalt and oxygen in the coated materials were recorded by ESCA (VG Scientific Escalab 250) in order to analyse the spatial distribution of the ions in the cathode particles.

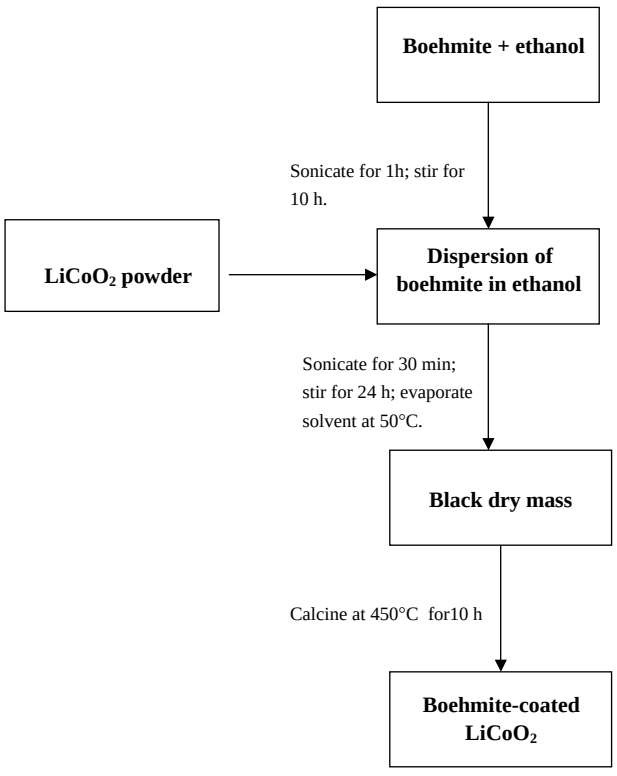

Fig. 1. Schematic of the mechano-thermal coating process.

Coin cells of the 2032 configuration were assembled in an argon-filled VAC MO40-1 glove box in which the oxygen and water contents were maintained below 2 ppm. Lithium metal (Foote Mineral) was used as the anode and a 1 M solution of $LiPF_6$ in EC:DEC (1:1 v/v) (Tomiyama Chemicals) was used as the electrolyte. The cathode was prepared by blade-coating a slurry of 85 wt % coated active material with 10 wt % conductive carbon black and 5 wt % poly(vinylidene fluoride) binder in *N*-methyl-2-pyrrolidone on an aluminium foil, drying overnight at 120 °C in an oven, roller-pressing the dried coated foil, and punching out circular discs. The cells were cycled at 0.1 or 0.2 *C* rate (with respect to a theoretical capacity of 274 mAh g^{-1}) between 2.75 and 4.40 V in a multichannel battery tester (Maccor 4000). Phase transitions occurring during the cycling processes were examined by a slow scan cyclic voltammetric experiment, performed with a three-electrode glass cell. The working electrodes were prepared with the cathode powders as described above, but coated on both sides of the aluminium foil. The cells for the cyclic voltammetric studies were assembled inside the glove box with lithium metal foil serving as both counter and reference electrodes. The electrolyte used was the same as that for the coin cell. Cyclic voltammograms were run on a Solartron 1287 Electrochemical Interface at a scan rate of 0.1 mVs^{-1} between 3.0 and 4.4 V.

3. Results and discussion

3.1. *X-ray diffraction*

The X-ray diffraction pattern of the boehmite coating material is shown in Figure 2. The diffraction pattern shows that the material is crystalline. The crystallite size of the boehmite sample, calculated with the Scherrer equation, was 2.98 nm. The BET surface area was

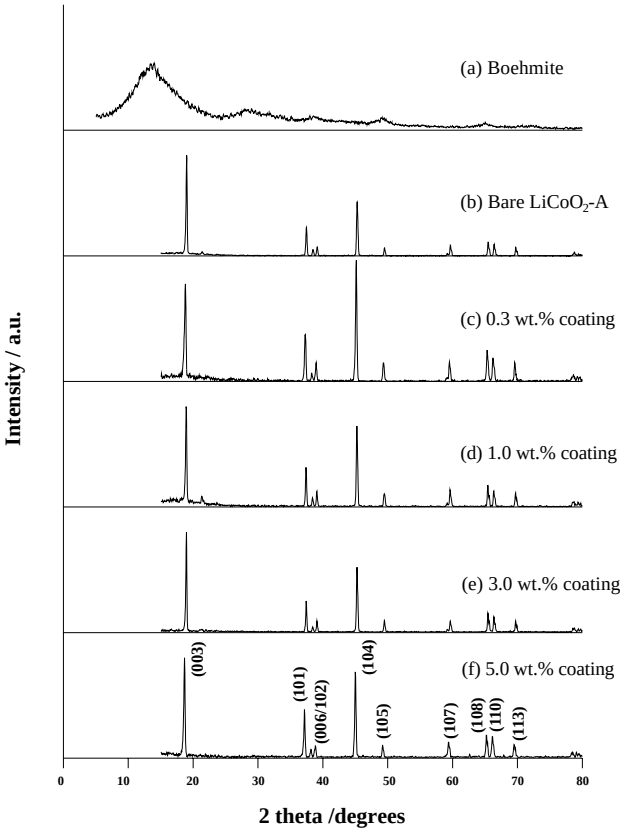

Fig. 2. X-ray diffraction patterns of the bare and coated $LiCoO_2$-A powders.

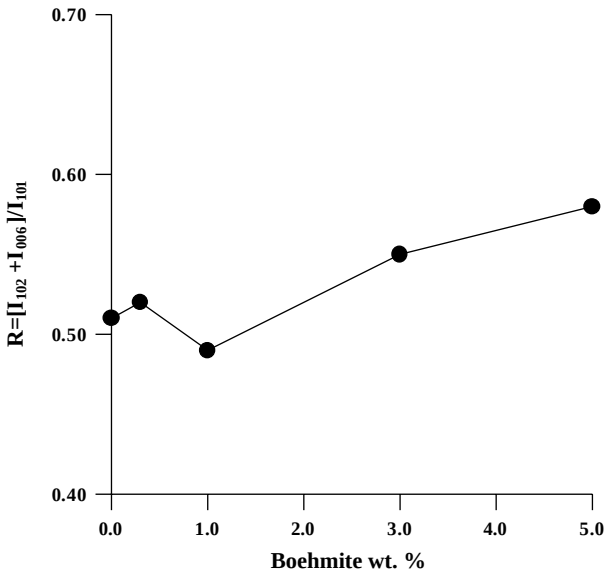

Fig. 3. Variation of the *R*-factor as a function of the coating level. Core material: $LiCoO_2$-A.

500 $m^2\ g^{-1}$. The particle size of boehmite, as obtained from DLS measurements, was about 10 nm.

The X-ray diffraction patterns of the bare and coated $LiCoO_2$ powders conform to the $R\bar{3}m$ symmetry of the core material. Typical patterns for boehmite-coated $LiCoO_2$-A sample are shown in Figure 2. The absence of any diffraction patterns corresponding to boehmite is attributed to the fact that the amount of coating material was small. Table 1 shows that the lattice constants *a* and *c* of the coated materials are less than those for the uncoated sample, suggesting that the phases on the surface of the powder are solid solutions formed by the reaction of the boehmite particles with the core material. It is possible that during the 10 h calcination process a substitutional compound $Li_xAl_yCo_{1-y}O_2$ could have formed through the interaction of the aluminium species with the substrate. The contraction in the *c* parameter indicates such a possibility. Co-substituted Al_2O_3 could also have formed, which means that the composition of the surface film is a complex mixture of the substituted oxides. Similar interoxide surface compositions have been proposed by other researchers too [11, 12, 14, 17–20]. Lithium diffusion occurs through this surface layer.

According to Dahn et al. [21, 22], the *R*-factor, defined as the ratio of the intensities of the hexagonal characteristic doublet peaks (006) and (102) to the (101) peak, is an indicator of hexagonal ordering. According to these authors, the lower the *R*-factor, the better the hexagonal ordering, and, hence, the electrochemical performance. The values of the *R*-factor were 0.51, 0.52, 0.49, 0.55 and 0.58 for coating levels of 0.0, 0.3, 1.0, 3.0 and 5.0 wt %, respectively (Figure 3). It can be seen that the *R*-value was lowest at the 1.0 wt % coating level. As seen below, the electrochemical behaviour of the coated samples generally reflects the above trend in the *R*-factor values.

3.2. *Morphology*

SEM images of the various coated $LiCoO_2$-A powders are shown in Figure 4. The texture of the cathode particle surface distinctly changed upon coating. The increased brightness of the materials observed in these

Table 1. Lattice constants and *R*-factor values of the bare and boehmite-coated $LiCoO_2$-A

Composition	*y*	*a*/Å	*c*/Å	*c*/*a*	*R*-factor	Unit cell volume/$Å^3$
(100-*y*) wt %	0.0	2.840	13.981	4.93	0.51	98.01
$LiCoO_2$-A + (*y*)	0.3	2.814	14.001	4.98	0.52	96.02
wt% boehmite	1.0	2.810	13.963	4.97	0.49	95.48
	3.0	2.807	13.932	4.96	0.55	95.07
	5.0	2.802	13.914	4.96	0.58	94.61

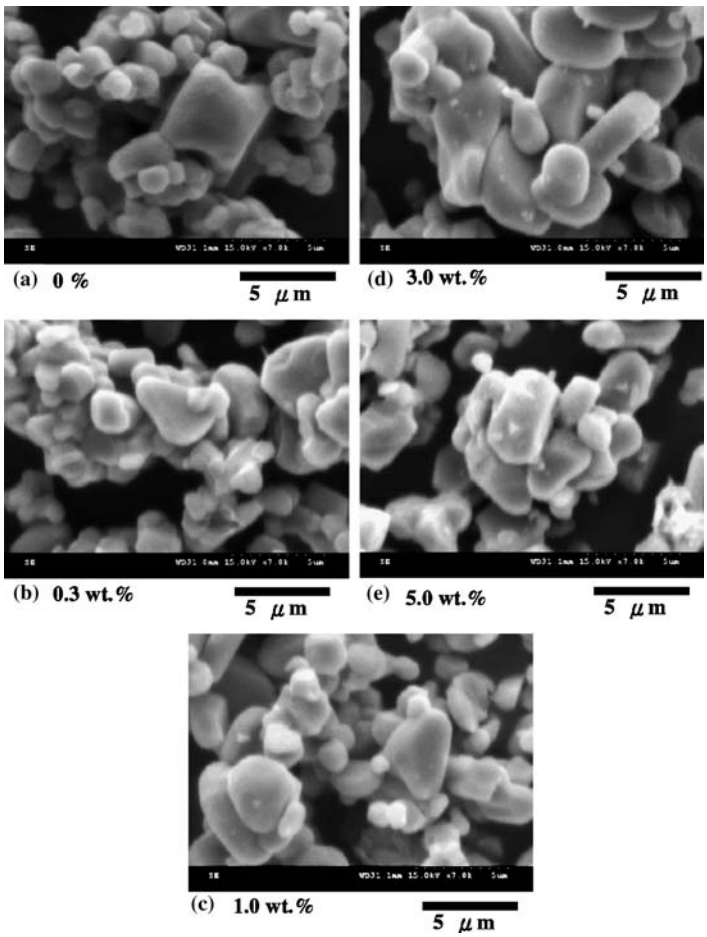

Fig. 4. SEM images of the various coated $LiCoO_2$-A powders.

pictures as the coating level increased is associated with the accumulation of charge on the non-conducting coating material as the electron beam impinges on it. It can be seen that at low concentrations (0.3 and 1.0 wt %) the coating is uniform. However, at higher coating levels small, loosely held agglomerates of the coating material are found glued to the surface, which suggests that at the 3.0 and 5.0 wt % coating levels, the amount of boehmite is more than what is required to form a uniform coating on the cathode powder, and that the excess silica agglomerates into small globules on the surface. Thus, it appears that a coating level of 1.0 wt % or less would be sufficient to impart a uniform coating on the cathode powder. Figure 5 shows the TEM image of a coated sample. The boehmite particles can be seen bound to the surface in the form of a distinguishable kernel, the thickness of which is around 20–30 nm. It is also conceivable that during the calcination process, some of the aluminium species might have diffused into the bulk, resulting in the formation of solid solutions. It is suggested that the chemical interaction between the core and the coating materials makes the coating more adherent.

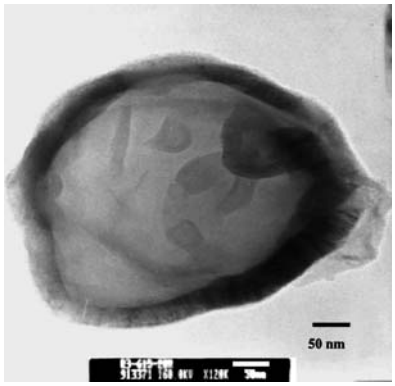

Fig. 5. TEM images of boehmite-coated $LiCoO_2$-A particles.

The BET surface areas of the bare and the 1.0 wt % coated $LiCoO_2$-A powders were 0.62 and 2.99 $m^2\ g^{-1}$. The higher surface area of the coated material is indicative of the larger specific surface area of boehmite. The surface area of boehmite was 500 $m^2\ g^{-1}$. Therefore, an increase in the surface area by about 2.4 $m^2\ g^{-1}$ is reasonable with a 1.0 wt % of boehmite particles distributed over the surface of the cathode particles, assuming that part of the coated particles form tightly bound interoxide compositions on the surface. Similarly, the surface area increased from 0.27 $m^2\ g^{-1}$ for the bare $LiCoO_2$-B sample to 1.91 $m^2\ g^{-1}$ when a coating of 1.0 wt % of boehmite was applied.

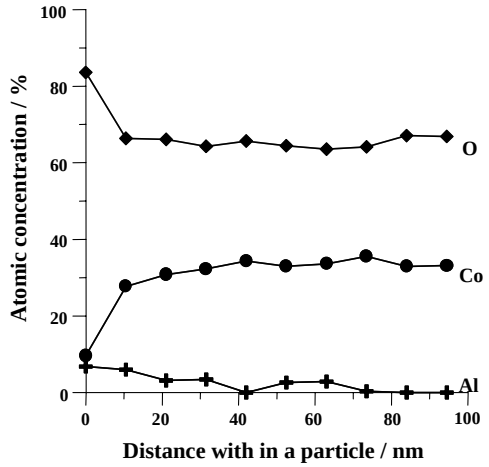

Fig. 6. ESCA depth profiles of aluminium, oxygen and cobalt in 1.0 wt % boehmite-coated $LiCoO_2$-A.

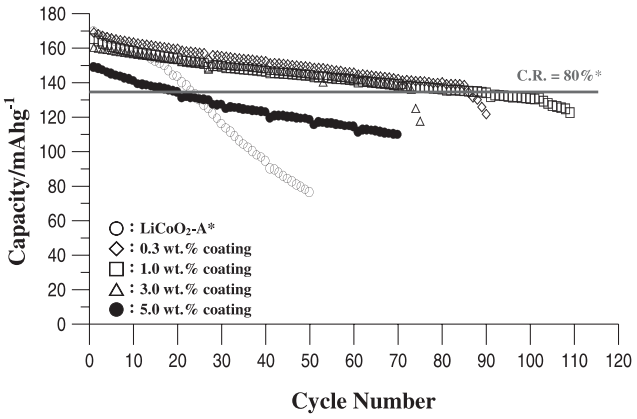

Fig. 7. Cycling behaviour of bare and various boehmite-coated LiCoO2-A samples. Charge–disharge: 0.2 C rate between 2.75 and 4.40 V.

3.3. *ESCA*

The spatial distribution of the coated material in the samples is displayed in the depth profiles presented in Figure 6. The high atomic concentration of oxygen at the surface of the oxide is understandable. The concentration of cobalt increased to a depth of about 20 nm and then levelled off. There was an attendant decrease in the aluminium concentration, which leveled off beyond 20 nm depth. The value of 20–30 nm in the depth profiles attributable to the coating layer is in agreement with the thickness of the coating as obtained from our TEM examination (Figure 5). Thus, it is clear that the surface of the particles was encapsulated in an aluminium-rich layer, and that any cobalt that may have been present on the surface is the result of a slow diffusion of the cations from the interior during the calcination process. As inferred from our XRD results, it is also possible that the cobalt on the surface may be part of the $Li_xAl_yCo_{1-y}O_2$ substitutional compound formed upon calcination. Based on the atomic concentrations of cobalt, oxygen and aluminium, a tentative composition of $Li_xAl_{0.2}Co_{0.8}O_2$ can be assigned for the material present at a depth of 10 nm in the coating.

3.4. *Galvanostatic cycling*

The galvanostatic cycling behaviour of the bare and coated $LiCoO_2$-A samples at a charge–discharge rate of 0.2 *C* is shown in Figure 7. The first-cycle discharge capacity of the bare $LiCoO_2$ sample was 169 mAh g^{-1}, while those of the 0.3, 1.0, 3.0 and 5 wt % coated samples were 169, 165, 160 and 149 mAh g^{-1}, respectively. Thus, the initial capacity was reduced as the coating level was increased. This is expected as the amount of active material in the cathode mix decreased as the coating level was increased. The larger drop in capacity at the high coating levels may have to do with the thickness of the coatings, which restricts the diffusion of lithium through the insulating layers. Additionally, the presence of excess coating material between the particles may lower the particle-to-particle electronic conductivity, and adversely affect the charging and discharging efficiencies.

As can be seen from Figure 7, the coating improved the cyclability of the cathode material. For a cut-off value of 80% for the capacity retention, calculated with the first-cycle discharge capacity of the uncoated material as the reference, the number of cycles that the bare $LiCoO_2$ could sustain was 23. The cyclability rose to 83 and 86 cycles, respectively, for the materials coated with 0.3 and 1.0 wt % boehmite. However, when the coating levels were increased further to 3.0 and 5.0 wt %, the cyclability reduced to 74 and 22, respectively. At the highest coating level employed (5.0 wt %), the fall in the cyclability was precipitous, consistent with the fact that the high amounts of the insulating boehmite would impede electronic conductivity between adjacent particles. The cyclability of the materials is roughly commensurate with the trend in the variation of the *R*-factor (Figure 3), which shows the lowest value for the *R*-factor at the 1.0 wt % coating level. The yclability also reflects the surface morphological features of the coated particles (Figure 4). According to Courtright [23], thinner coatings produce smaller cracks that are a factor in controlling the ingress of molecular species. At the optimum coating level (1.0 wt %), the cathode material registered nearly a three-fold increase in cyclability (from 23 to 86 cycles).

The low-rate (0.1 *C*) cycling behaviour of boehmite-coated $LiCoO_2$-A samples is shown in Figure 8. The cut-off capacity was fixed at 80% of the first-cycle discharge capacity of the bare material. It can be seen that the number of cycles that the bare sample could sustain before reaching the cut-off value increased to 30. At the optimum coating level of 1.0 wt %, the cyclability at the lower rate was also higher, the material sustaining as many as 100 cycles. This represents a three-fold improvement in cyclability.

Coated $LiCoO_2$-B samples were also tested at the higher discharge rate (0.2 *C*). The results are presented

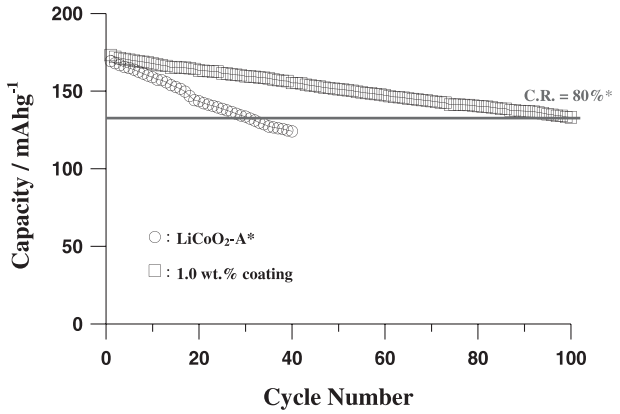

Fig. 8. Cycling behaviour of bare and 0.1 wt % boehmite-coated $LiCoO_2$-A samples. Charge–discharge: 0.1 *C* rate between 2.75 and 4.40 V.

in Figure 9. The bare sample sustained only 13 cycles before 20% of its capacity was lost. Again, the 1.0 wt % coated material gave the best performance, sustaining 160 cycles. This represents a remarkable twelve-fold increase in cyclability. Compared to the boehmite-coated $LiCoO_2$-A samples, the performance improvement is greater with the coated $LiCoO_2$-B samples. At the same charge-discharge rate (0.2 *C*), the material that gave a lower number of cycles in its bare form ($LiCoO_2$-B: 13 cycles) registered a larger improvement upon coating than did the one that sustained 23 cycles in its bare form. Thus, although boehmite coating helped increase the cyclability of $LiCoO_2$, the effect seems to vary with the core cathode material used. The reason for the difference in the extent of improvement is presently not obvious. Although variations in the surface areas and particle sizes of the two cathode materials have been noted (Section 2), a thorough understanding on the effect of the nature of the core material on the cyclability enhancement would call for a separate study. However, the mechano-thermal coating process opens up the possibility of improving the cyclability of commercial and already well-cycling cathode materials. Moreover, the process is attractive for commercial adaptability for reasons of economics and simplicity of procedures.

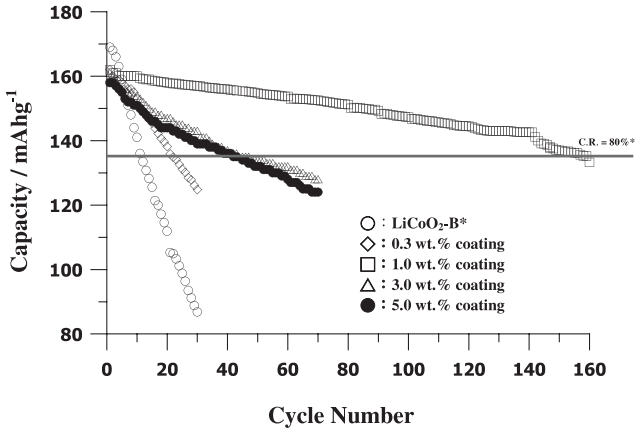

Fig. 9. Cycling behaviour of bare and various boehmite-coated $LiCoO_2$-B samples. Charge–discharge: 0.2 *C* rate between 2.75 and 4.40 V.

3.5. *Cyclic voltammetry*

$LiCoO_2$ undergoes structural transitions at potentials above 4 V, which can significantly impinge on the cycling stability of the cathode. For example, during charging, a transition from the hexagonal phase (H) to a monoclinic phase (M) occurs around 4.1 V, which further transforms into a hexagonal phase around 4.2 V vs Li^+/Li [24]. Accompanying these phase transitions is a 1.2% expansion of the lattice in the *c*-direction, which is considered to be above the limit of ~0.1% in elastic strain that oxides can tolerate [25]. Repeated phase transitions upon cycling can lead to 'electrochemical grinding' by which microcracks are generated in the particles, resulting in enhanced capacity fades.

Slow scan cyclic voltammetry was performed to examine the effect of the coating on the phase transitions that accompany the charge–discharge processes. Figure 10(a) shows the cyclic voltammograms of bare $LiCoO_2$-A while Figure 10(b) presents those for 1.0 wt % boehmite-coated $LiCoO_2$-A. The large peak around 3.95 V in the first sweep during the charging of the cathode is due to the deintercalation of lithium accompanied by the oxidation of Co^{3+} to Co^{4+}. The small current peaks that follow are attributed to transitions from the hexagonal to monoclinic phase and again to the hexagonal phase. During the reverse sweep, re-intercalation takes place between 3.85 and 3.80 V. It can be seen that as the cycling progresses, the

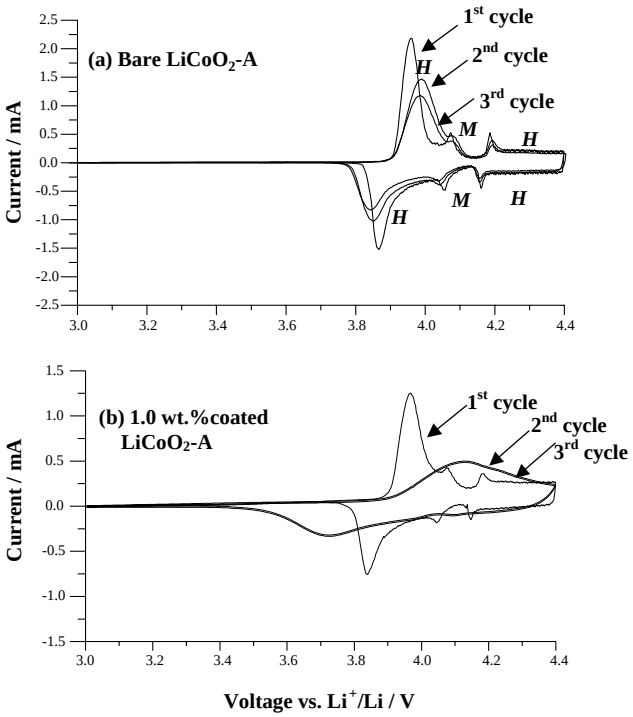

Fig. 10. Cyclic voltammograms of (a) bare $LiCoO_2$-A (b) 1.0 wt % boehmite-coated $LiCoO_2$-A.

redox peak shifts slightly to higher potentials in the forward sweep shift, and to lower potentials in the reverse sweep. This suggests a progressive increase in the overpotentials for the corresponding reactions. In the case of the coated cathodes, it appears that the peaks shift only between the first and second cycles; from then on the shift is insignificant. This suggests good reversibility of the charge–discharge processes from the second cycle onwards for the coated cathode materials.

It can be seen from the cyclic voltammograms that the peaks for the lithium insertion process shift to lower potentials upon coating. This reflects the charge–discharge profiles of the bare and coated materials (Figure 11). The shift to lower potentials suggests that the surface oxide aids in the diffusion of lithium from the core material. The beneficial effect of aluminium as a dopant on the structural characteristics of $LiCoO_2$ is well known [11, 26, 27]. The charging curves in Figure 11 show that the deintercalation potentials for the coated materials were higher than those for the bare material. This can be likened to the case of aluminium-doped $LiCoO_2$ cathodes, for which a higher charging voltage is observed [28], as predicted by *ab initio* calculations of Ceder et al. [29, 30]. Thus, aluminium-containing surface oxides lead not only to structural stability of the core cathode, but also to the formation of aluminium-rich insulating surface oxides upon charging [31], which is beneficial as protection against overcharge.

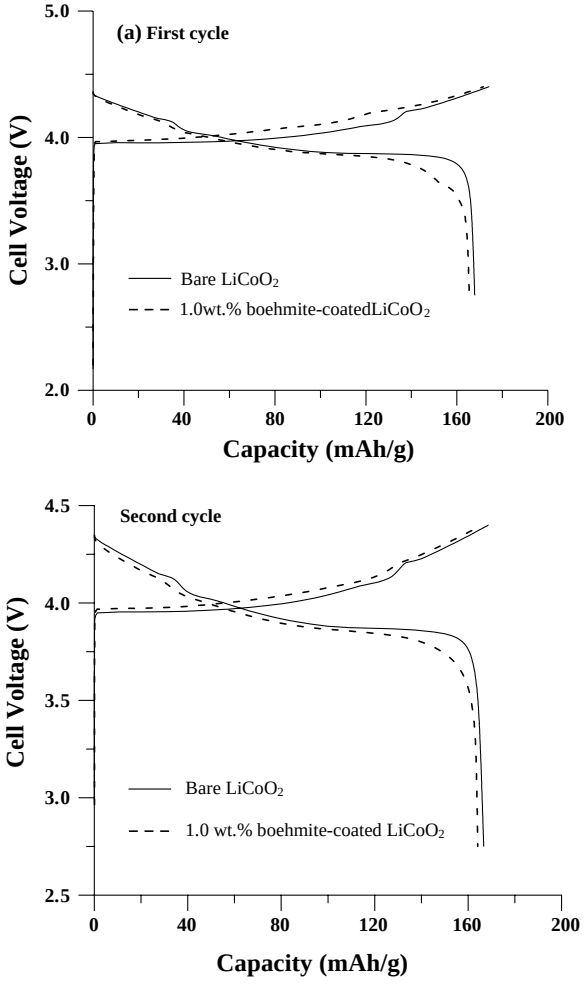

Fig. 11. Galvanostatic charge–discharge curves for the bare and 1.0 wt % boehmite-coated $LiCoO_2$: (a) first cycle; (b) second cycle.

It can be seen that the H–M–H phase transitions persist through the cycling in the bare material (Figure 10(a)). Although the first run of the cyclic voltammogram of the 1.0 wt %-coated material showed hardly any change compared to the cyclic voltammogram of the bare sample, the peaks corresponding to the phase transitions are suppressed from the second cycle onwards (Figure 10(b)). It is possible that any defect in the coating is repaired upon repeated cycling. The presence of cracks, pinholes, and other coating defects on coated surfaces is inevitable. It is conceivable that such defects may form and close with the application of a load, or upon thermal cycling. In our case, changes in the surface texture that occurred as a result of the contraction and expansion of the lattice during the cycling process may have enabled the nanoparticulate coating material to become ingrained in the crevices and cracks on the cathode surface. The resulting more compact kernel led to suppression of phase transitions, thus enhancing the cyclability of the coated material. According to Cho et al. [13], a fracture-tough oxide kernel over $LiCoO_2$ can suppress volume changes accompanying the cycling processes. In fact, it can be seen from Figure 10(b) that from the second cycle onwards, the cyclic voltammogram of the boehmite-coated material shows little evidence of such a transformation even at 4.4 V vs Li^+/Li.

A comparison of Figures 10 and 11 show that there is a correspondence between the plateaus of the charge–discharge profiles and the peaks in the cyclic voltammograms. The large plateaus (or peaks) around 3.9 V″ are due to the coexistence of two pseudo-phases of $LiCoO_2$, one a lithium-deficient phase and the other, a lithium-rich phase [32]. The two small plateaus (or peaks) in the figures for the bare cathode correspond to the order–disorder phase transitions occurring around $x = 0.5$ in $Li_{1-x}CoO_2$ [6]. The corresponding plateaus for the coated material are not obvious in their charge–discharge curves. Thus, it is clear that the aluminium-containing coating suppresses the phase transitions. Cho et al. [11], found that a coating of Al_2O_3 on $LiCoO_2$ reduces the cation disorder, which the authors ascribe to a suppression of the hexagonal-to-monoclinic phase transitions [11]. One of the reasons for capacity fade in $LiCoO_2$ is the reaction of the electrolyte with the highly oxidizing Co^{4+} formed during charging [33]. The adherent and inert coating on the surface of the cathode particles prevents direct contact of the cathode with the electrolyte, enhancing the cyclability.

4. Conclusions

Preformed boehmite nanoparticles were coated on commercial $LiCoO_2$ cathode samples by a simple

mechano-thermal coating process. Although the XRD patterns of the coated materials did not show any extraneous peaks corresponding to the coated particles, the slightly lower interlayer distance, *c*, observed with the coated samples showed that a substitutional compound of the composition $Li_xAl_yCo_{1-y}O_2$ might have formed on the surface. SEM images showed the presence of small spherules of boehmite glued to the coated cathode particles at 3.0 and 5.0 wt % coating levels, suggesting that such coating levels are above what is required for a uniform coating. TEM images revealed a kernel of about 20–30 nm thickness on the cathode particles. ESCA depth profiles showed the presence of aluminium up to about 20 nm, suggesting that a surface interoxide composition might have formed. Cycling studies showed that at a coating level of 1.0 wt %, the improvement in cyclability was the greatest. The lowest *R*-factor value for this material supports the good structural stability of the 1.0 wt %-coated sample, which confers the high cyclability. At a charge–discharge rate of 0.2 *C*, a 1.0 wt % coating of boehmite particles enhanced the cyclability three-fold and twelve-fold for samples $LiCoO_2$-A and $LiCoO_2$-B, respectively. The variation in performance improvement with the core material opens up possibilities for applying this method to enhance the cyclability of already well-cycling cathode materials. Furthermore, because of its simplicity and economics, the mechano-thermal process described here holds much potential for commercial adaptability.

Acknowledgements

Financial support for this work from the Industrial Technology Research Institute and National Science Council (NSC) is gratefully acknowledged. TPK and SPN thank the NSC of the Republic of China for the award of post-doctoral fellowships.

References

1. L.D. Dyer, B.S. Borie, Jr. and G.P. Smith, *J. Am. Chem. Soc.* **76** (1954) 1499.
2. J.P. Parant, R. Olazcuga, M. Devalette, C. Fouassier and P. Hagenmuller, *J. Solid State Chem.* **3** (1971) 1.
3. C. Fouassier, G. Matejka, J. M. Reau and P. Hagenmuller, *J. Solid State Chem.* **6** (1973) 532.
4. K. Mizushima, P.C. Jones, P.J. Wiseman and J.B. Goodenough, *Mater. Res. Bull.* **15** (1980) 783.
5. J.B. Goodenough, K. Mizushima and T. Takeda, *Jpn. J. Appl. Phys.* **19** (1980) 305.
6. J.N. Reimers and J.R. Dahn, *J. Electrochem. Soc.* **139** (1992) 2091.
7. T. Ohzuku and A. Ueda, *J. Electrochem. Soc.* **141** (1994) 2972.
8. H.F. Wang, Y.I. Jang, B.Y. Huang, D.R. Sadoway and Y.M. Chiang, *J. Electrochem. Soc.* **146** (1999) 473.
9. E. Plichita, S. Slane, M. Uchiyama, M. Salomon, D. Chua, W.B. Ebner and H.W. Lin, *J. Electrochem. Soc.* **136** (1989) 1865.
10. G.G. Amatucci, J.M. Tarascon and L.C. Klein, *Solid State Ionics* **83** (1996) 167.
11. J. Cho, Y.J. Kim and B. Park, *Chem. Mater.* **12** (2000) 3788.
12. J. Cho, Y.J. Kim and B. Park, *J. Electrochem. Soc.* **148** (2001) A1110.
13. J. Cho, Y.J. Kim, T-J. Kim and B. Park, *Angew. Chem. Int. Ed.* **40** (2001) 3367.
14. X. Wang, L. Liu, L. Chen and X. Huang, *Solid State Ionics* **148** (2002) 335.
15. M. Mladenov, R. Stoyanova, E. Zhecheva and S. Vassilev, *Electrochem. Comm.* **3** (2001) 410.
16. Z. Wang, C. Wu, L. Liu, F. Wu, L. Chen and X. Huang, *J. Electrochem. Soc.* **149** (2002) A466.
17. J. Cho, C-S. Kim and S-I. Yoo, *Electrochem. Solid-State Lett.* **3** (2000) 362.
18. J. Cho, G.B. Kim, H.S. Lim, C-S. Kim and S-I. Yoo, *Electrochem. Solid-State Lett.* **2** (1999) 607.
19. H-J. Kweon, S.J. Kim and D.G. Park, *J. Power Sources* **88** (2000) 255.
20. H-J. Kweon and D.G. Park, *Electrochem. Solid-State Lett.* **3** (2000) 128.
21. J.N. Reimers, E. Rossen, C.D. Jones and J.R. Dahn, *Solid State Ionics* **61** (1993) 335.
22. J.R. Dahn, U. von Sacken and C.A. Michal, *Solid State Ionics* **44** (1990) 87.
23. E.L. Courtright, *Surf. Coat. Technol.* **68–69** (1994) 116.
24. H.F. Wang, Y.I. Jang, B.Y. Huang, D.R. Sadoway and Y.M. Chiang, *J. Electrochem. Soc.* **146** (1999) 473.
25. L.H. van Vlack, 'Physical Ceramics for Engineers' (Addison-Wesley, Reading, MA, 1964).
26. Y-I. Jang, B. Huang, H. Wang, D.R. Sadoway, G. Ceder, Y-M. Chiang, H. Liu and H. Tamura, *J. Electrochem. Soc.* **146** (1999) 862.
27. L. Liu, Z. Wang, H. Li, L. Chen and X. Huang, *Solid State Ionics* **152** (2002) 341.
28. W-S. Yoon, K-K. Lee and K-B. Kim, *J. Power Sources* **97–98** (2001) 303.
29. M.K. Aydinol, A.F. Kohan, G. Ceder, K. Cho and J. Joannopoulos, *Phys. Rev. B solid state* **56** (1997) 1354.
30. G. Ceder, Y-M. Chiang, D.R. Sadoway, M.K. Aydinol, Y-I. Jang and B. Huang, *Nature* **392** (1998) 694.
31. J. Kim and K. Amine, *J. Power Sources* **104** (2002) 33.
32. Y.M. Choi, S.I. Pyun, J.S. Bae and S.I. Moon, *J. Power Sources* **56** (1995) 25.
33. D. Zhang, B.S. Haran, A. Durairajan, R.E. White, Y. Podrazhansky and B.N. Popov, *J. Power Sources* **91** (2000) 122.